THE JOURNAL OF BIOLOGICAL CHEMISTRY
Vol. 280, No. 15, Issue of April 15, pp. 15131–15140, 2005
Printed in U.S.A.

Structures of *Escherichia coli* NAD Synthetase with Substrates and Products Reveal Mechanistic Rearrangements*

Received for publication, November 22, 2004, and in revised form, January 26, 2005
Published, JBC Papers in Press, February 7, 2005, DOI 10.1074/jbc.M413195200

Ralf Jauch‡, Andreas Humm§, Robert Huber¶, and Markus C. Wahl‖**

From the ‡Max-Planck-Institut für Biophysikalische Chemie, Abteilung Molekulare Entwicklungsbiologie, Am Fassberg 11, D-37077 Göttingen, Germany, §Roche Diagnostics GmbH, Nonnenwald 2, 82372 Penzberg, Germany, ¶Max-Planck-Institut für Biochemie, Strukturforschung, Am Klopferspitz 18a, D-82152 Martinsried, Germany, and ‖Max-Planck-Institut für Biophysikalische Chemie, Abteilung Zelluläre Biochemie/Röntgenkristallographie, Am Fassberg 11, D-37077 Göttingen, Germany

Nicotinamide adenine dinucleotide synthetases (NADS) catalyze the amidation of nicotinic acid adenine dinucleotide (NAAD) to yield the enzyme cofactor nicotinamide adenine dinucleotide (NAD). Here we describe the crystal structures of the ammonia-dependent homodimeric NADS from *Escherichia coli* alone and in complex with natural substrates and with the reaction product NAD. The structures disclosed two NAAD/NAD binding sites at the dimer interface and an adenosine triphosphate (ATP) binding site within each subunit. Comparison with the *Bacillus subtilis* NADS showed pronounced chemical differences in the NAAD/NAD binding sites and less prominent differences in the ATP binding pockets. In addition, the *E. coli* NADS structures revealed unexpected dynamical rearrangements in the NAAD/NAD binding pocket upon NAAD-to-NAD conversion, which define a catalysis state and a substrate/product exchange state. The two states are adopted by concerted movement of the nicotinysyl moieties of NAAD and NAD, Phe-170, and residues 224–228, which may be triggered by differential coordination of a magnesium ion to NAAD and NAD. Phylogenetic structure comparisons suggest that the present results are relevant for designing species-specific antibiotics.

Nicotinamide adenine dinucleotide (NAD)[1] is a ubiquitous carrier of reduction equivalents and functions as a cofactor in numerous metabolic reactions. NAD plays further roles in processes as diverse as calcium mobilization, DNA repair, and post-translational modification of proteins in eukaryotes. The final step of NAD biosynthesis is catalyzed by the enzyme NAD synthetase (NADS) and involves the conversion of nicotinic acid adenine dinucleotide (NAAD) to NAD (1) (see Fig. 1*A*). NAD synthetase activity was first described in the late 1950s (2, 3). Two types of NADS enzymes have been discovered; the first using preferentially ammonia as the amide donor, the second employing glutamine instead. The corresponding reaction schemes have been reported in 1967 (4).

$$ATP + NAAD + NH_3 \rightarrow AMP + PP_i + NAD$$

REACTION 1

$$ATP + NAAD + \text{L-glutamine} \rightarrow AMP + PP_i + NAD + \text{L-glutamate}$$

REACTION 2

In the course of the above reactions, the enzymes mediate an adenylyl transfer from ATP to the nicotinysyl moiety of NAAD, resulting in NAD-adenylate (see Fig. 1*B*) as a reaction intermediate. The second step of the reaction is the amidation of the nicotinysyl moiety using either ammonia (Reaction 1) or glutamine (Reaction 2) as an amide source.

NADSs from several prokaryotes, including *Bacillus subitilis* (*bsu*) (5), *Escherichia coli* (*eco*) (6, 7), and *Mycobacterium tuberculosis* (*mtu*) (8) have been cloned and characterized. Both *eco*NADS and *bsu*NADS exhibit a clear preference for ammonia over glutamine (2, 5, 7), whereas the *mtu*NADS can use both glutamine and ammonia as amide donors (8). Recently, the human (NADsyn1, here referred to as NADS1) and yeast (Qns1) NADSs have been characterized (9–11). Eukaryotic NADSs confer an additional N-terminal domain with nitrilase activity, which enables them to use glutamine as an amide donor (10).

NADS from *Bacillus subtilis* has been subjected to intensive crystallographic investigations. At first, the crystal structures of the *bsu*NADS apoenzyme, the complex of *bsu*NADS with ATP, and the complex of *bsu*NADS with the reaction intermediate NAD-adenylate had been reported (12–14). Subsequently, the picture was expanded by co-crystallizing *bsu*NADS with NAAD, AMP + PP_i (a combination of NAAD and ATP), and also with the ATP analog AMP-CPP (15). More recently, a 1.0-Å resolution structure of *bsu*NADS in complex with the NAD-adenylate intermediate has been described (16). The combined structural studies unraveled the overall architecture of a NADS and delineated its mode of substrate binding. They defined separate binding sites for the ATP co-substrate (ATP binding pocket) and the substrate NAAD (NAAD/NAD binding pocket), and they revealed some details of the catalytic mechanism. NADS blocking agents have been suggested to be promising antibiotics for pathogens, such as *Bacillus anthracis*, which may be developed employing the *bsu*NADS crystal structures (17, 18).

In the present study, we provide high resolution crystal structures of NADS from *E. coli*, which shed light on evolutionary relationships among the enzymes *eco*NADS and *bsu*NADS.

* This work was supported by the Max-Planck-Society. The costs of publication of this article were defrayed in part by the payment of page charges. This article must therefore be hereby marked "*advertisement*" in accordance with 18 U.S.C. Section 1734 solely to indicate this fact.

The atomic coordinates and structure factors (codes 1WXE, 1WXF, 1WXG, 1WXH, and 1WXI) have been deposited in the Protein Data Bank, Research Collaboratory for Structural Bioinformatics, Rutgers University, New Brunswick, NJ (http://www.rcsb.org/).

** To whom correspondence should be addressed: Max-Planck-Institut für Biophysikalische Chemie, Abteilung Zelluläre Biochemie/Röntgenkristallographie, Am Fassberg 11, D-37077 Göttingen, Germany. Tel.: 49-551-201-1046; Fax: 49-551-201-1197; E-mail: mwahl@gwdg.de.

[1] The abbreviations used are: NAD, nicotinamide adenine dinucleotide; NADS, NAD synthetase; NAAD, nicotinic acid adenine dinucleotide; AMP-CPP, adenosine 5′-(α,β-methylene)triphosphate; PDB, Protein Data Bank.

In addition to the structure of the apoenzyme and complexes of the enzyme with AMP, NAAD, and AMP+PP_i, we present also the structure of NADS in association with its reaction product, NAD. This structure exhibits some unexpected rearrangements both in the active site and in the product molecules upon conversion of NAAD to NAD. The results reveal novel dynamical aspects for the reaction mechanism for ammonia-dependent NADSs. This work should also aid in the design of species-specific inhibitors for this class of enzymes.

EXPERIMENTAL PROCEDURES

Cloning, Expression and Purification—The *E. coli nadE* gene encoding NADS was PCR-amplified with *E. coli* DH5α cells as the template source and was inserted into the EcoRI site of the expression plasmid pRSETHE (derived from pRSET6d (19)). The expression product was designed to contain an N-terminal hexahistidine tag (tag sequence MAHHHHHHEF). The DNA construct was verified by automated sequencing, which predicted a protein product in accordance with SwissProt accession number P18843.

The protein was expressed in shaking cultures of *E. coli* BL21(DE3) cells at 32 °C overnight by the addition of 1 mM isopropyl-β-D-thiogalactopyranoside during the mid-log phase of growth. The cells were harvested by centrifugation, resuspended in buffer A (50 mM Tris-HCl, pH 7.0, 100 mM NaCl, 0.2 mM phenylmethylsulfonyl fluoride) and lysed by sonification (Branson sonifier, Schwäbisch Gmünd, Germany). The His-tagged protein was captured on a nickel-nitrilotriacetic acid column (Qiagen, Düsseldorf, Germany) in buffer A, washed with buffer B (50 mM Hepes-NaOH, pH 7.0, 100 mM NaCl, 50 mM imidazole, 0.2 mM phenylmethylsulfonyl fluoride), and eluted in a linear gradient to buffer C (50 mM Hepes-NaOH, pH 7.0, 100 mM NaCl, 800 mM imidazole, 0.2 mM phenylmethylsulfonyl fluoride). The NADS-containing fractions were pooled, dialyzed against buffer D (30 mM Hepes-NaOH, pH 8.0, 0.1 mM EDTA) and applied to a DEAE-cellulose column (DE-52, Whatman, Brentford, UK), washed with buffer E (20 mM Tris-HCl, pH 8.0), and eluted in a linear gradient to buffer F (20 mM Tris-HCl, pH 8.0, 400 mM NaCl). NADS eluted in the first of two peaks. The enzyme fractions were pooled, dialyzed against crystallization buffer (20 mM Tris-HCl, pH 7.0, 10 mM NaCl, 0.2 mM dithiothreitol, 0.2 mM EDTA), and concentrated by ultrafiltration (10-kDa molecular mass cutoff membrane; Amicon, Billerica, MA) to ~19 mg/ml.

Crystallization and Data Collection—*E. coli* NADS apoenzyme was crystallized in hanging drops by vapor equilibration at room temperature against 12.5–18.5% polyethylene glycol 400, 50 mM $MgCl_2$, 100 mM sodium acetate, pH 5.0–5.4, with a drop volume ratio of 2:1 (protein solution:reservoir). The addition of 1 μl of a suspension of lithium-*meta*-tantalate significantly increased the nucleation rate and quality of the crystals. Crystals appeared and grew within a period of 1–14 days. NADS-ligand complexes were obtained by co-crystallization, adding 1.5–2 mM AMP (form II), ATP (form III), NAAD (form IV), or NAD (form V) to the setup (Table I).

Diffraction data were recorded at room temperature with a Rigaku (Tokyo, Japan) rotating anode x-ray generator equipped with a MarResearch (Hamburg, Germany) image plate. For data collection, crystals were mounted in thin walled special glass capillaries (Charles Supper Company, Natick, MA) with mother liquor on one side. Data were processed using the HKL software package (20).

Structure Solution and Refinement—The *E. coli* NADS-NAD co-crystal structure was solved by molecular replacement with the AMoRe software program (21) using the *B. subtilis* NADS coordinates (Protein Data Bank (PDB) code 1NSY) as a search model. The molecular replacement solution was subjected to rigid body refinement and simulated annealing using crystallography and NMR system (CNS) software package (22). The model was further improved by alternating cycles of manual model building using the XtalView software program (23) and positional and temperature factor refinement steps (CNS). During refinement, clear difference density appeared for the cofactor, which was manually inserted (XtalView). During the last cycles of refinement, water molecules were built automatically (CNS) into spherical peaks of the $F_o - F_c$ difference electron density and verified by manual inspection. During all refinement steps, 5% of the reflections were set aside to monitor the free *R*-factor.

All other NADS structures were subsequently solved by molecular replacement using the *E. coli* NADS coordinates as a search model and refined as outlined above. The final geometries of the models were evaluated using the PROCHECK program (24). For structure analyses, various programs from the Uppsala software factory (x-ray.bmc.uu.se/usf/) and from the Collaborative Computational Project Number 4 (CCP4) program package (25) were employed. Coordinates and structure factors have been submitted to the Protein Data Bank (PDB codes 1WXE, 1WXF, 1WXG, 1WXH, 1WXI) and will be released upon publication.

RESULTS

Structure Solution and Quality of the Models—Recombinant *eco*NADS was produced, purified, and crystallized as described under "Experimental Procedures." The crystal structures of the *eco*NADS apoenzyme (form I; Table I) as well as four co-crystal structures with natural substrates and catalytic products (AMP, form II; AMP+PP_i, form III; NAAD, form IV; and NAD, form V; Table I) were solved by Patterson rotation/translation searches, using the structure coordinates of *bsu*NADS (PDB code 1NSY). The crystals of the enzyme complexes were obtained by co-crystallization and pertained to two different crystal systems (Table I). Employing diffraction data to maximum resolutions between 1.7 and 2.3 Å without intensity cutoffs, the models were refined to R_{work} and R_{free} values between 17.1 and 22.3%, maintaining good stereochemistry (Table I). All crystals comprised the full-length protein (residues 2–275), excluding the first methionine. No residues for the N-terminal hexahistidine affinity tag could be located in the electron densities. The short flexible loop P1 (residues 88–90) was not visible in the structures in which the ATP binding site is empty (forms I, IV, and V). A large loop P2 (residues 208–224; Fig. 2) could not be traced in either of the five crystal structures. Arg-186, located in a loop between β5 and α8 (see below for a description of the topology), exhibited a disallowed dihedral angle conformation in all five models, which was maintained because of unambiguous $2F_o - F_c$ electron density for this residue. The unusual conformation is stabilized through hydrogen bonds and ionic interactions with Glu-22, Ser-26, Pro-183, and Leu-184.

Global Structure and Comparison to the B. subtilis Enzyme—*eco*NADS exhibits an α/β fold similar to the *B. subtilis* enzyme (Figs. 3 and 4*A*). 55% of all residues are found in α-helical conformation, 15% belonging to β-structures. A twisted five-stranded parallel β-sheet is sandwiched between the two large helices α3 and α6. All β-strands are separated by single α-helices, with the exception of β3 and β4, which are disrupted by two α-helices (α5 and α6). Thus, the core of *eco*NADS comprises a typical Rossmann fold nucleotide binding motif.

In both space groups, C2 and $P3_121$, *eco*NADS or its complexes crystallized with one protein molecule per crystallographic asymmetric unit. It has been well established that bacterial NADSs form homodimers (7, 12). In the present crystals, *eco*NADS monomers are positioned close to crystallographic two-fold axes, which generate the functional dimers. The globular NADS homodimer has approximate dimensions of 77 × 60 × 56 Å. Based on an analysis with the protein-protein interaction server (26), ~2500 Å^2 of combined surface area are buried in the dimer interface, encompassing 18% of the solvent-exposed surface area of the molecules. Contacts between the protomers are principally mediated by the α5–α6 region. The two pairs of helices align homotypically in an antiparallel fashion (Fig. 3). The dimer interface is predominantly nonpolar (75% of the participating residues) and involves 14 hydrogen bonds but lacks intervening water molecules. Therefore, *eco*NADS qualifies as an obligatory dimer.

*eco*NADS and *bsu*NADS are 55% identical in their amino acid sequences (Fig. 2). Consistently, they exhibit quite similar overall folds. Fig. 4*A* shows an overlay of the NAAD-containing models from both organisms, which exhibit an average root mean square deviation of 0.55 Å for 241 aligned C-α atoms. Five regions in the *E. coli* protein contain more than one residue deviating by >1 Å from the *B. subtilis* structure (Fig. 4*A*): region 1 (residues 37–42) (*E. coli* numbering), region 2

TABLE I
Crystallographic data

Data in parentheses for the last 0.05 Å (for form I last 0.1 Å).

Crystals					
Form	I	II	III	IV	V
Cofactor	—[c]	AMP	AMP + PP_i	NAAD	NAD
Space group	$P3_121$	C2	C2	C2	$P3_121$
Unit cell parameters					
a (Å)	91.9	92.5	92.4	92.4	92.2
b (Å)	91.9	67.8	67.9	67.8	92.2
c (Å)	76.3	48.3	48.4	48.2	76.2
α (°)	90	90	90	90	90
β (°)	90	104.5	104.2	104.4	90
γ (°)	120	90	90	90	120
PDB ID code	1WXF	1WXE	1WXI	1WXG	1WXH
Data collection					
Resolution (Å)	30.0–2.3	30.0–1.8	30.0–1.7	30.0–1.9	30.0–1.9
Unique reflections	16,081	25,734	29,229	21,526	29,775
Redundancy	5.4	3.7	3.8	3.6	3.8
Completeness (%)	95.1 (97.7)	95.9 (92.1)	91.6 (87.6)	94.5 (91.7)	99.5 (95.3)
$I/\sigma(I)$	14.4 (3.0)	13.0 (2.9)	14.7 (2.7)	11.9 (2.3)	19.6 (3.0)
R_{sym}[a] (%)	8.8 (45.9)	10.8 (41.8)	7.4 (42.8)	11.7 (58.6)	5.4 (36.7)
Refinement					
Resolution	30.0–2.3	30.0–1.8	30.0–1.7	30.0–1.9	30.0–1.9
Reflections used	16080	25734	29229	21526	29758
Protein molecules/asymmetric unit	1	1	1	1	1
Protein atoms	2008	2029	2051	2008	2008
Solvent atoms	165	257	277	227	302
Nucleotide atoms	—	46	55	44	44
Mg^{2+}	—	1	2	1	1
R_{work}/R_{free}[b] (%)	18.3/21.7	19.1/21.1	17.6/20.5	19.9/22.3	17.1/19.1
Average temperature factors ($Å^2$)					
Protein	36.4	18.7	18.9	20.3	28.2
Water oxygens	47.8	33.9	38.1	34.2	50.4
Nucleotide (NAD/ATP sites)	—/—	19.5/45.1	17.1/38.6	29.0/—	38.3/—
Mg^{2+}	—	42.9	59.2	33.5	—
Wilson *B*-factor	38.9	26.5	26.8	24.5	33.3
Root mean square deviation from ideal values					
Bond length (Å)	0.005	0.005	0.005	0.005	0.005
Bond angle (°)	1.08	1.20	1.10	1.13	1.15
Ramachandran analysis					
Preferred (%)	93.6	93.9	93.9	94.5	92.3
Additionally allowed (%)	6.0	5.7	5.3	5.0	7.3
Disallowed (%)	0.4	0.4	0.8	0.5	0.4

[a] $R_{sym}(I) = (\Sigma_{hkl}\Sigma_i[|I_i(hkl) - \langle I(hkl)\rangle|]/\Sigma_{hkl}\Sigma_i[I_i(hkl)]$; $I_i(hkl)$ − intensity of the ith measurement of hkl; $\langle I(hkl)\rangle$ − average value of hkl for all i measurements.

[b] $R_{work} = \Sigma_{hkl}[||F_{obs}| - k|F_{calc}||]/\Sigma_{hkl}[|F_{obs}|]$; $R_{free} = \Sigma_{hkl\subset T}[||F_{obs}| - k|F_{calc}||]/\Sigma_{hkl\subset T}[|F_{obs}|]$; $hkl\subset T$ − test set.

[c] —, not determined.

(residues 71–76), region 3 (residues 125–129), the far C terminus, and the C-terminal continuation of the P2 loop. Regions 1 and 2 exhibit single or double amino acid insertions in *eco*NADS. Significantly, region 1 is intimately involved in binding of the adenylyl moiety in the NAAD/NAD binding pocket (see below). In contrast, the deviating regions 2, 3, and the far C terminus are distant from the substrate binding sites and are therefore not expected to exhibit effects on the substrate or product binding characteristics of the enzymes. The P2 loop has a fundamental impact on the catalytic mechanism (see "Architecture of the NAAD/NAD Binding Site").

Design of the ATP Binding Site—In the present ensemble of crystal structures, the ATP binding sites of form II and III crystals contained AMP and AMP+PP_i, respectively, whereas the site was empty in the apoenzyme (form I), in the NAAD complex (form IV), and in the NAD complex (form V). Crystal form III was obtained by the addition of ATP to the crystallization drops, but the crystals contained AMP and pyrophosphate, indicating that hydrolysis of ATP took place during crystallization.

Each of the two ATP binding sites in the *eco*NADS dimer is formed exclusively from one subunit. In crystal forms II and III, the ribose portions of the adenine nucleotides are engaged in hydrogen bonding interactions with the backbone oxygen of Gly-46 (to ribose O-2′) and the side chain hydroxyl group of Thr-160 (to ribose O-3′). The AMP adenine ring is held in place through stacking interactions with Arg-142, Ile-47, and Ser-48 (Fig. 5*A*). A hydrogen bond between N-6 of the adenine moiety and Gln-88 leads to a stabilization of loop P1, as indicated by clear $2F_o - F_c$ electron density for this protein region. In contrast, no electron density developed for loop P1 in the apoform or in other crystals with unoccupied ATP binding sites (forms I, IV, and V). Flexibility in loop P1 is the only recognizable mechanism to yield access to the ATP binding site. Thus, the P1 loop serves as a lid, which is flexibly designed to allow ATP access but closes the ATP pocket upon substrate binding.

The side chain of Arg-82 exists in two conformations in the AMP co-crystal structures. In the major conformation, it interacts either with Gln-88 of the P1 loop and with N-1 of the adenine moiety. In the minor conformation, it interacts with the side chains of Glu-91 and Gln-95 from helix α4 (Fig. 5*A*). The latter conformation of Arg-82 is the only form seen in crystal structures with unoccupied ATP binding sites (forms I, IV, and V). The conformation of Arg-82, in which it interacts with Gln-88 and the adenine of the nucleotide, thus seems to be induced upon ATP/AMP binding. Because the other conformation of Arg-82, in which it interacts with helix α4 residues and which is characteristic of the nucleotide-free state, is seen as a minor conformation in the AMP and AMP+PP_i co-crystal structures; a small portion of the protein molecules in these latter crystals presumably have no nucleotide bound. Taken together, Arg-82 in *eco*NADS seems to play the role of a sub-

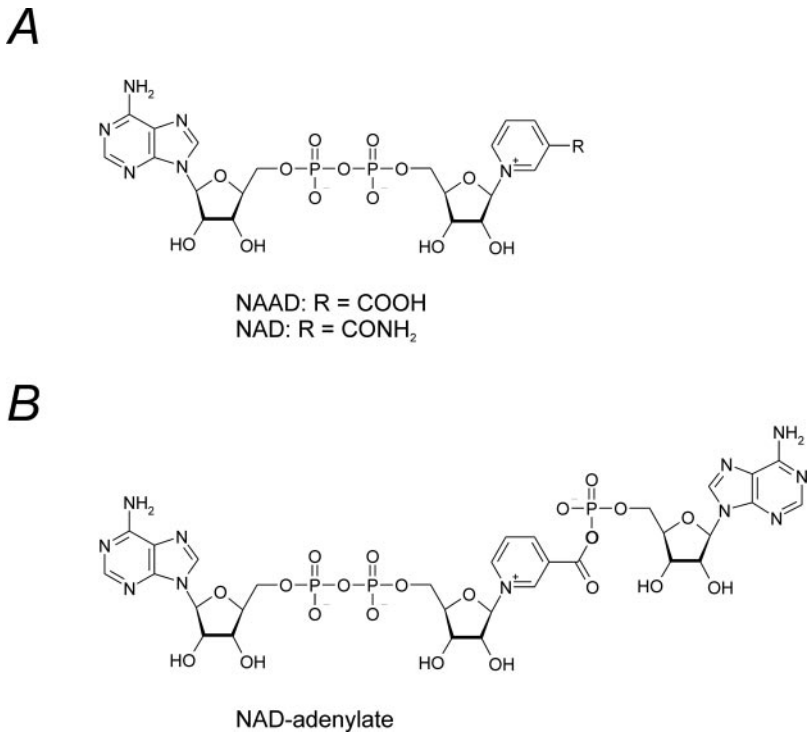

FIG. 1. **Chemical structures.** *A*, structure of the reaction substrate (NAAD) and product (NAD). *B*, structure of the reaction intermediate NAD-adenylate.

strate sensor or gate keeper for the ATP binding pocket.

As in most ATP-binding proteins, several magnesium ion binding sites have been reported for *bsu*NADS (14). In the present *eco*NADS structures, a Mg^{2+} binding site (site I) is clearly occupied as well in crystal forms II (AMP), III (AMP+PP_i), and IV (NAAD), *i.e.* in structures that contain at least AMP at the ATP binding site or NAAD at the NAAD/NAD binding site. The Mg^{2+}-I ions show a typical octahedral coordination sphere, which in the AMP+PP_i co-crystal structure (form III) is composed of oxygens from the AMP α-phosphate, the two phosphate groups of the pyrophosphate moiety (former β- and γ-phosphates of ATP), the side chain carboxyls of Asp-51 and Glu-165 and a water molecule (Fig. 5*C*). In the AMP co-crystal structure (form II), which lacks the pyrophosphate molecule, and in the NAAD co-crystal structure (form IV), in which the ATP binding pocket is unoccupied, missing phosphate oxygens are replaced by water molecules in the coordination sphere.

In crystals of form IV (NAAD co-crystal), the nicotinysyl portion of NAAD is oriented toward Mg^{2+}-I. The nicotinysyl carboxyl group of NAAD is engaged in a hydrogen bond with a water oxygen, which belongs to the octahedral coordination sphere of Mg^{2+}-I (Fig. 5*C*). The latter water oxygen coincides with the position of an α-phosphate oxygen in forms II (AMP) and III (AMP+ PP_i) structures. In contrast, the form V structure (NAD co-crystal) does not contain the Mg^{2+}-I ion. Correlating with this observation, the nicotinysyl moiety of NAD is differently oriented from the corresponding portion of NAAD and is pointing away from the Mg^{2+}-I binding site (see "Architecture of the NAAD/NAD Binding Site"). Therefore, in the NAAD co-crystal structure, Mg^{2+}-I is seen as a direct link between the ATP binding pocket and the NAAD/NAD binding pocket. This direct interaction is lost upon formation of the product NAD.

A second magnesium ion (Mg^{2+}-II) has been reported in *bsu*NADS crystal structures (14, 15), where it is coordinated by the AMP α-phosphate, two pyrophosphate oxygens, two water molecules, and the backbone carbonyl oxygen of Thr-208 (*B. subtilis* numbering). In the present ensemble of structures, the Mg^{2+}-II ion is only seen in form III crystals (AMP+PP_i complex). Because Mg^{2+}-II is present only in the AMP+PP_i complex, the pyrophosphate (or by inference the β- and γ-phosphate groups of ATP) is required to capture a magnesium ion at site II in *eco*NADS.

Comparison of the ATP Binding Sites of E. coli and B. subtilis NADS—Ordering of the P1 loop upon occupation of the ATP binding site has also been seen in *bsu*NADS. Therefore, loop P1 seems to be a conserved flexible element, the function of which is to close the ATP binding site upon the addition of a nucleotide. In *eco*NADS, we have observed an additional conformational change in the side chain of Arg-82 upon AMP+PP_i binding, which is consistent with Arg-82 constituting a sensor for the occupation of the ATP pocket (Fig. 5*A*). In contrast, according to available models for the *B. subtilis* protein, the Arg-82 conformation of the nucleotide-bound forms is preformed in the *bsu*NADS apoenzyme. Thus, despite a high degree of similarity in the chemical composition of the ATP binding pockets, *eco*NADS and *bsu*NADS seem to respond differently to nucleotide binding.

Significantly, in *bsu*NADS, the N-terminal part of loop P2 contributes the backbone carbonyl oxygen of Thr-208 (*B. subtilis* numbering) for coordination of Mg^{2+}-II in the ATP binding pocket. Loop P2 is ordered in structures of the *Bacillus* enzyme, in which nucleotides occupy the ATP pocket, portraying how this region can fold back onto the bulk of the protein (Fig. 4*B*). In contrast, loop P2 is disordered in the present structures of *eco*NADS. The sequence of loop P2 is highly conserved between the two enzymes, and *eco*NADS also comprises a threonine residue corresponding to Thr-208^{bsu} (Thr-210^{eco}; superscripts identify the organism). However, although the AMP+PP_i co-crystal structure (form III) of *eco*NADS contains a Mg^{2+}-II, the backbone of the P2 loop remains disordered. It is possible that one ligand of the Mg^{2+}-II coordination sphere in the *eco*NADS form III structure, which has been modeled as a water molecule, actually corresponds to the backbone carbonyl of Thr-210^{eco} and that the P2 loop becomes partially ordered upon occupation of the Mg^{2+}-II site. However, full ordering of the P2 loop seems to be supported by crystal packing contacts. In the

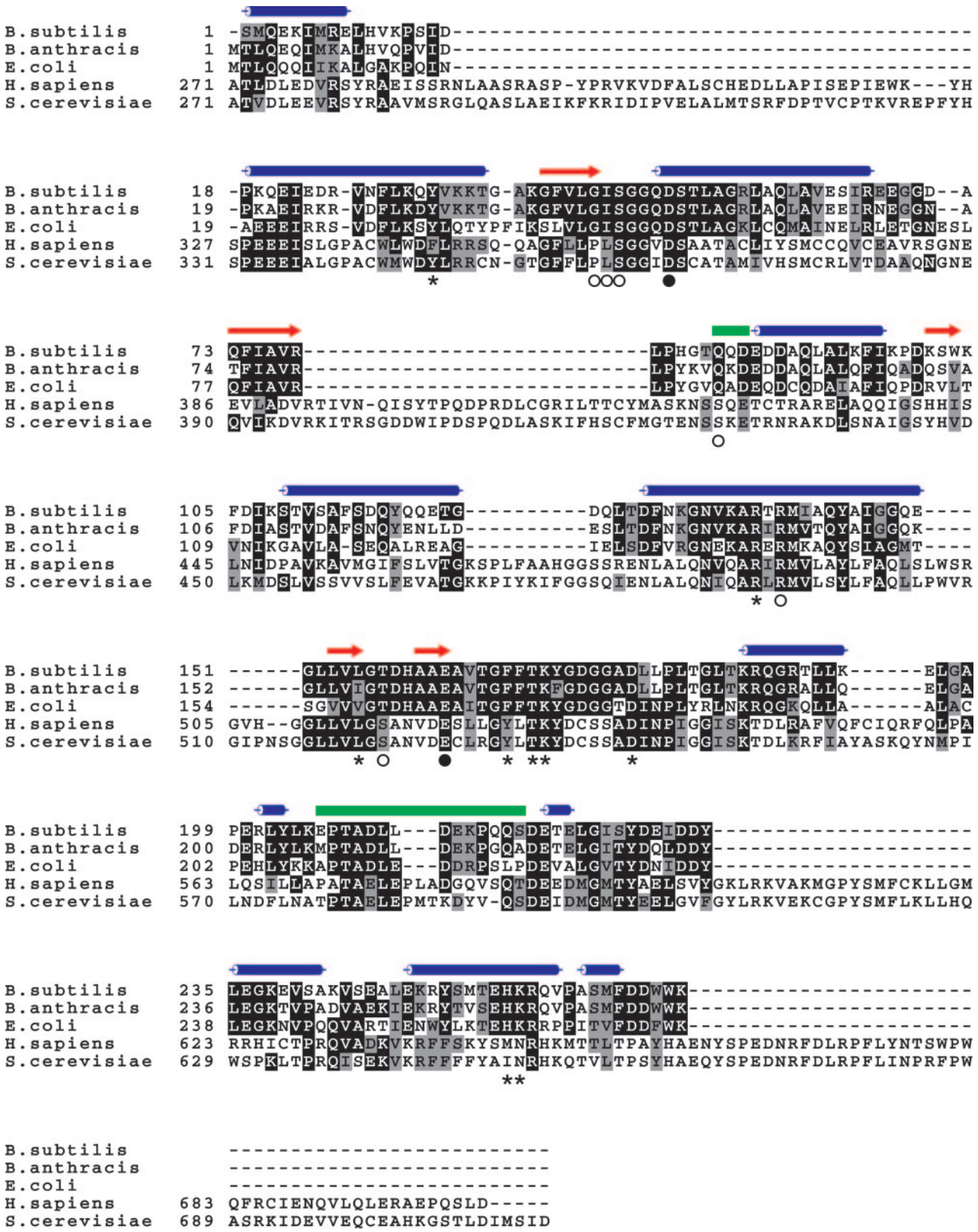

FIG. 2. **Sequence alignment.** Alignment of *B. subtilis, B. anthracis, E. coli*, human (NADsyn1) and *Saccharomyces cerevisiae* (Qnsp1) NADSs. Human and yeast proteins comprise a number of insertions. An additional N-terminal domain in these proteins, not found in the bacterial NADSs, has been omitted from the alignment. *Asterisks* highlight residues involved in NAD/NAAD binding in bacteria. *Closed circles* indicate residues involved in the coordination of Mg^{2+}-I, and *open circles* indicate residues, which interact with ATP at the ATP site. *Blue* helix *icons above the alignment* denote α-helices, and *red arrows* denote β-strands as found in the *eco*NADS structure. *Green bars above the alignment* denote loops P1 (residues 88–90 of *eco*NADS) and P2 (residues 209-222) The alignment was generated using the ClustalW program (www.ebi.ac.uk/clustalw/).

*bsu*NADS crystal structures, residues Glu-214^{bsu} and Lys-215^{bsu} from the central portion of loop P2 are involved in salt bridges to a neighboring molecule of the crystal lattice. In contrast, the P2 region in both *eco*NADS crystal systems (C2 and $P3_121$) faces a large solvent channel, creating a solution-like environment around this region of the enzyme.

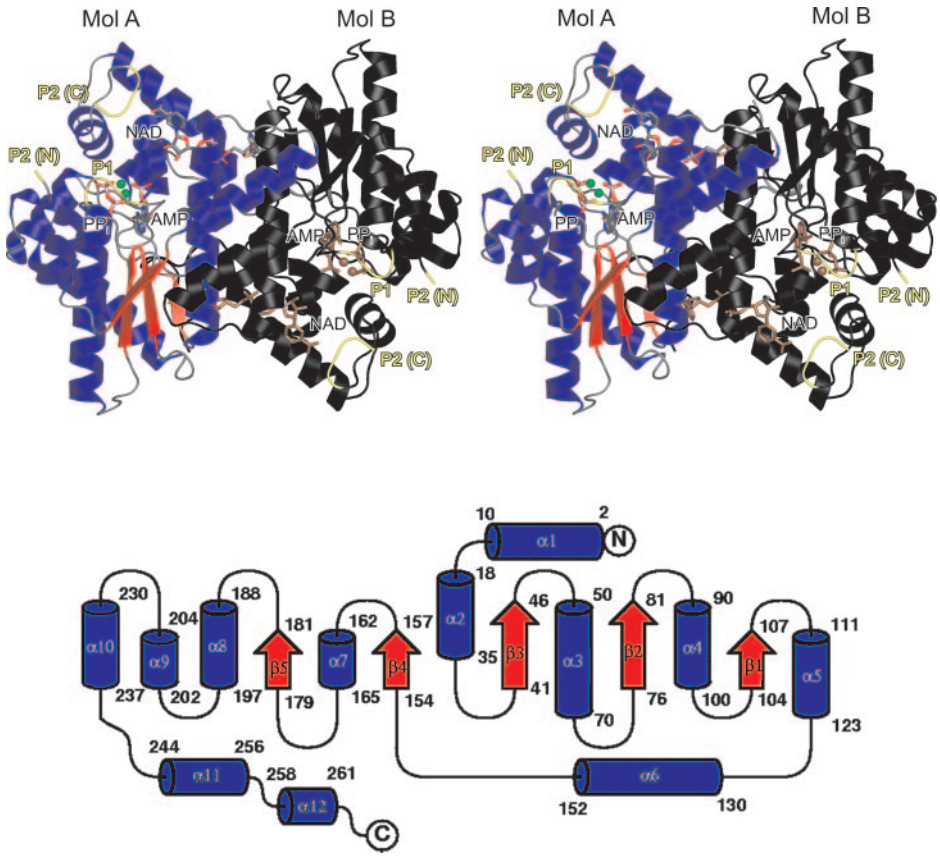

FIG. 3. **Overall structure of *eco*NADS.** *Upper panel*, stereo ribbon plot of an *E. coli* NADS homodimer. One NADS molecule (*Mol A*) is color-coded by secondary structure (α-helices in *blue*, β-strands in *red*, and loops in *gray*). The other (*Mol B*) is shown in *black*. Flexible loops P1 and P2 are shown in *yellow*. To indicate the respective binding pockets, NAD, AMP, and PP_i (as found in different crystal structures) are shown as *stick figures*. Mg^{2+} ions are indicated as *spheres*. Cofactors of molecule A are color-coded by atom type (carbon in *gray*, oxygen in *red*, nitrogen in *blue*, phosphorus in *pink*, and magnesium in *green*). Cofactors of molecule B are in *brown*. By default, structure figures were generated using the PyMOL program (pymol.sourceforge.net/). *Lower panel*, topology plot generated with Ligplot (27). *N*, N terminus; *C*, C terminus.

In conclusion, we note that the N-terminal part of loop P2 can adopt various degrees of ordering, completely fixed (as in the structures of *bsu*NADS with nucleotides in the ATP pocket), partially ordered (as in the structure of AMP+PP_i of *eco*NADS), and completely disordered (as in the structures of *eco*NADS, in which β- and γ-phosphates are lacking from the ATP binding site). To some degree, ordering of loop P2 thus seems to be dependent upon occupation of the Mg^{2+}-II site, the fixation of which in turn depends on the presence and mode of binding of the ATP β- and γ-phosphates or, after hydrolysis, the PP_i leaving group. The interplay between the second Mg^{2+} ion and the N-terminal part of loop P2 therefore correlates with the state of the nucleotide in the ATP binding pocket.

Architecture of the NAAD/NAD Binding Site—The two identical NAAD/NAD binding sites per homodimer are located at the dimer interface (Fig. 3). Both subunits provide residues for NAAD/NAD binding (in the following termed subunit A and subunit B). In the present structures, we observed three different nucleotides at the NAAD/NAD binding site: AMP in forms II (AMP co-crystallization) and III (ATP co-crystallization), NAAD in form IV, and NAD in form V. Thus, co-crystallization in the presence of adenine nucleotides (but without NAD or NAAD) leads to the occupation of the NAAD/NAD binding site by AMP.

Binding of the adenosyl portions of the nucleotides by the enzyme is identical in the co-crystal structures with NAAD (form IV) and NAD (form V), and the adenosyl parts are tightly fixed at the dimer interface by these interactions. The adenine ring of the AMP portion of the nucleotides is sandwiched between His-260 from subunit A and Ile-40/Val-156 from subunit B. Tyr-33^B (superscripts identify the subunit) is engaged in a hydrogen bonding interaction with the adenine N-1 atom. The adenylyl ribose interacts via its 3′-OH with Asp-180^B (carbonyl oxygen) and via O-4′ with His-260^A (atom $N^{\epsilon 2}$). The phosphate groups interact with the side chains of Lys-261^A, Arg-140^A, and Asn-136^A and with the backbone nitrogen of Lys-173^A.

In contrast, the nicotinysyl parts of both NAAD and NAD are fixed to a lesser extent compared with the adenosyl parts, indicated by higher temperature factors. However, the conformation of both NAAD and NAD could be unambiguously determined in $F_o - F_c$ "omit" electron density maps (Fig. 5*B*). The nicotinic acid ring of NAAD is stabilized by the side chains of Phe-170^A, Thr-172^A, and Asp-176^A. The NAD conformation in form V crystals deviates significantly from the NAAD conformation (Fig. 3*C*). Relative to the NAAD structure, the nicotinamide moiety of NAD is rotated around the O-5′–C-5′ bond (Fig. 5*C*). Supporting the alternate NAD conformation, Phe-170 undergoes a concomitant structural change, from stacking on the NAAD nicotinysyl ribose to stacking with the nicotinamide ring of NAD (Fig. 5*C*). The conformation of Phe-170 in the apoenzyme structure resembles its preferred conformation in the NAD co-crystal structure. In contrast, the structures of *eco*NADS, in which AMP is bound to the NAD site (forms II and III), exhibit a NAAD-like Phe-170 conformation.

The conformation of loop P2 also appears to be subjected to rearrangements in the course of the enzymatic reaction. Although loop P2 could be traced neither in the form IV (NAAD) nor in the form V (NAD) structures as mentioned above, the conformation of the residues 224–228, which comprise the first traceable part after the disordered stretch 208–223, is strikingly different in the NAD complex compared with the NAAD co-crystal structure (Fig. 5*C*). The regions of the two structures exhibit C-α root mean square deviation values of >3 Å. Resembling the behavior of Phe-170, the conformation of region 224–228 in form V (NAD) recalls the conformation of the apoform (form I), whereas its conformation in form IV (NAAD) is highly similar to the models with occupied ATP sites (forms II and III). Significantly, the preferred conformation of NAD in the NAAD/NAD pocket and the conformation of the surrounding enzyme

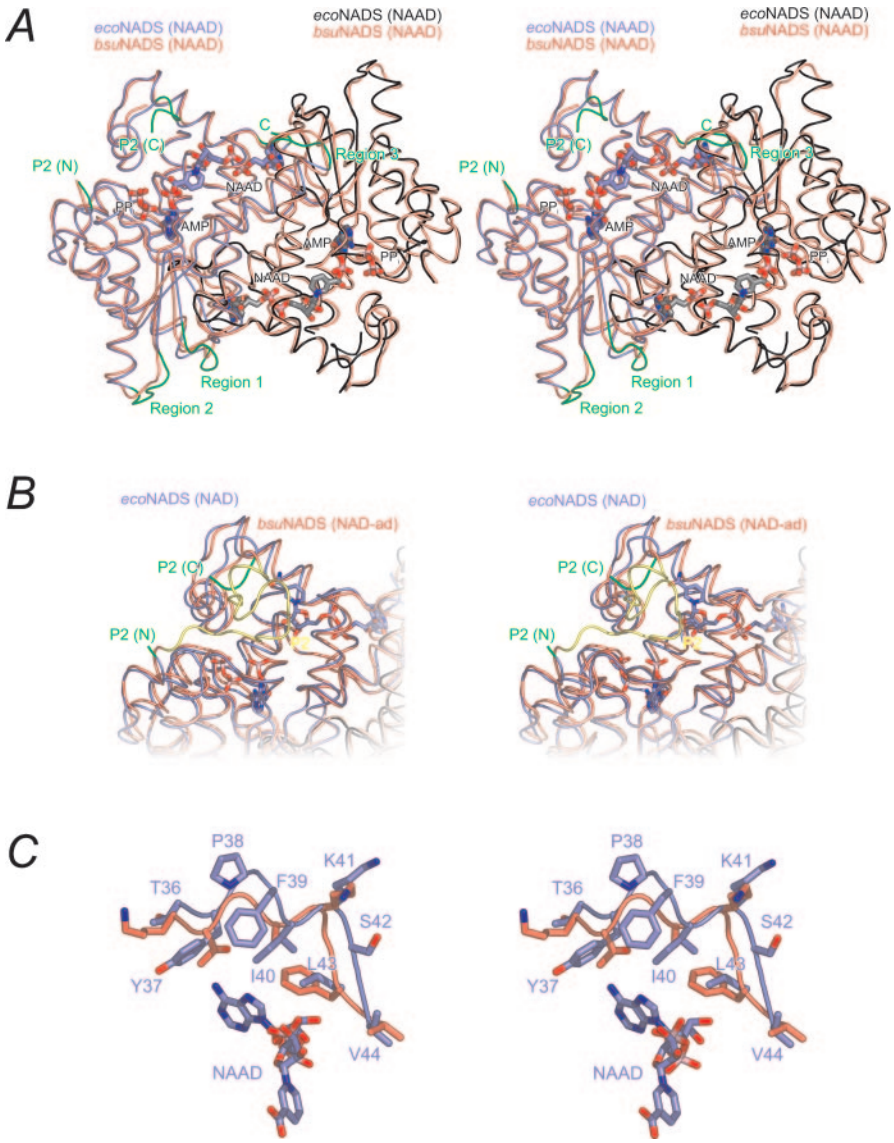

FIG. 4. **Phylogenetic comparison.** *A*, stereo view of a superpositioning of the NAAD co-crystal structures of *E. coli* NADS (*ecoNADS*) (*left* subunit in *light blue* and *right* subunit in *black*) and *B. subtilis* NADS (*bsuNADS*) (both subunits in *red*; PDB code 1IFX). The NADS homodimers are shown in the same orientation as in Fig. 3. Cofactors are indicated by *broad sticks* (color-coded by atom type: oxygen in *red*, nitrogen in *blue*, and phosphorus in *pink*). Carbons for ligands of the *left* subunit are *light blue*, and those for ligands of the *right* subunit are *gray*). Besides NAAD, which was co-crystallized with the enzymes shown, AMP and PP_i from the form III crystal structure are superimposed to indicate the ATP binding pockets. Regions with a C-α root mean square deviation >1 Å between the two enzymes are colored in *green* in the *left* subunit of *eco*NADS (region 1, residues 36–41; region 2, residues 70–75; region 3, residues 124–128). *B*, detailed stereo view of a similar superpositioning of *eco*NADS (NAD complex) with *bsu*NADS (NAD-adenylate complex), indicating residues for the P2 loop in *yellow* (*bsu*NADS) and for residues neighboring the P2 loop in *green* (*eco*NADS). Other coloring and the orientation of the figure are identical to those of the *left* subunit in *A*. *C*, comparison of region 1 from the two enzymes, which contains residues close to the NAAD/NAD binding site after global superpositioning of the molecules. Atoms are color-coded by type as above. Carbons and backbone traces of *eco*NADS are shown in *light blue*, and those of *bsu*NADS are in *red*. Residues of *eco*NADS are labeled in *single letter* style. The NAAD molecules superimpose almost perfectly; therefore, only one (from *eco*NADS) is shown for clarity.

regions (Phe-170 and residues 224–228) in the NAAD co-crystal structure, and vice versa, are mutually exclusive. Superposition of the NAD-*eco*NADS and NAAD-*eco*NADS co-crystal structures clearly show a sterical hindrance for adoption of the NAAD-bound conformation of region 224–228 when NAD is present and vice versa (Fig. 5*C*). In this regard, it is important to note that the change in conformation of *eco*NADS region 224–228 and of Phe-170 also correlates with the presence of Mg^{2+}-I, which we have shown above to be involved in orientation of the substrate NAAD, but which is lacking when NAD is present. Therefore, release of AMP+PP_i and concomitant loss of Mg^{2+}-I may be involved in the adoption of the NAD/apoform structures of the enzyme.

In conclusion, two alternative states of the NAAD/NAD binding site exist in *eco*NADS, represented by alternative conformations observed for Phe-170, residues 224–228 (and most likely the remainder of the P2 loop), and the nicotinysyl moieties of NAAD and NAD, as well as the differential coordination of NAAD and NAD to Mg^{2+}-I. One conformation, which is observed in the apoform and in the NAD-bound form of the enzyme and which we term the "exchange (E) state," seems to allow substrate binding and product release. The other conformation, which is formed upon occupation of the ATP binding site or in the presence of the substrate NAAD and which we term the "catalysis (C) state," has to be adopted for substrate conversion. It is noteworthy that these differences affect both the ATP binding pockets and the NAAD/NAD binding pockets and are therefore indicative of a structural communication between these sites during catalysis.

Comparison to the NAAD/NAD Binding Site of bsuNADS—Region 1, pointed out in the global comparison above (Fig. 4*A*), provides the docking environment for the adenylyl moiety in the NAAD/NAD binding site (Fig. 4*C*). Its amino acid composition is decisively different in *eco*NADS and *bsu*NADS (Figs. 2 and 4*C*). *E. coli* region 1 contains a higher number of bulky, hydrophobic, or aromatic residues: Tyr-37 instead of Thr, Pro-38 instead of Gly, a Phe-39 insertion and Ile-40 instead of Ala (Figs. 2 and 4*C*). Despite these chemical differences, similar binding of the adenylyl moiety of NAAD or NAD is achieved by the two enzymes. Because of the phylogenetic variability in region 1, the NAAD/NAD pocket may be of particular interest for the development of species-specific antibiotics. Additional minor variations at the NAD binding environment, such as the replacement of Val-156 and Trp-256 in *eco*NADS by Leu-153 and Arg-253 in *bsu*NADS, could be of further relevance for rational inhibitor design.

We have outlined above how the N-terminal portion of loop P2 (residues 208–224) is involved in nucleotide binding at the ATP site through coordination of the Mg^{2+}-I ion. In *bsu*NADS, Ala-209 and Leu-211 from the same region of the P2 loop

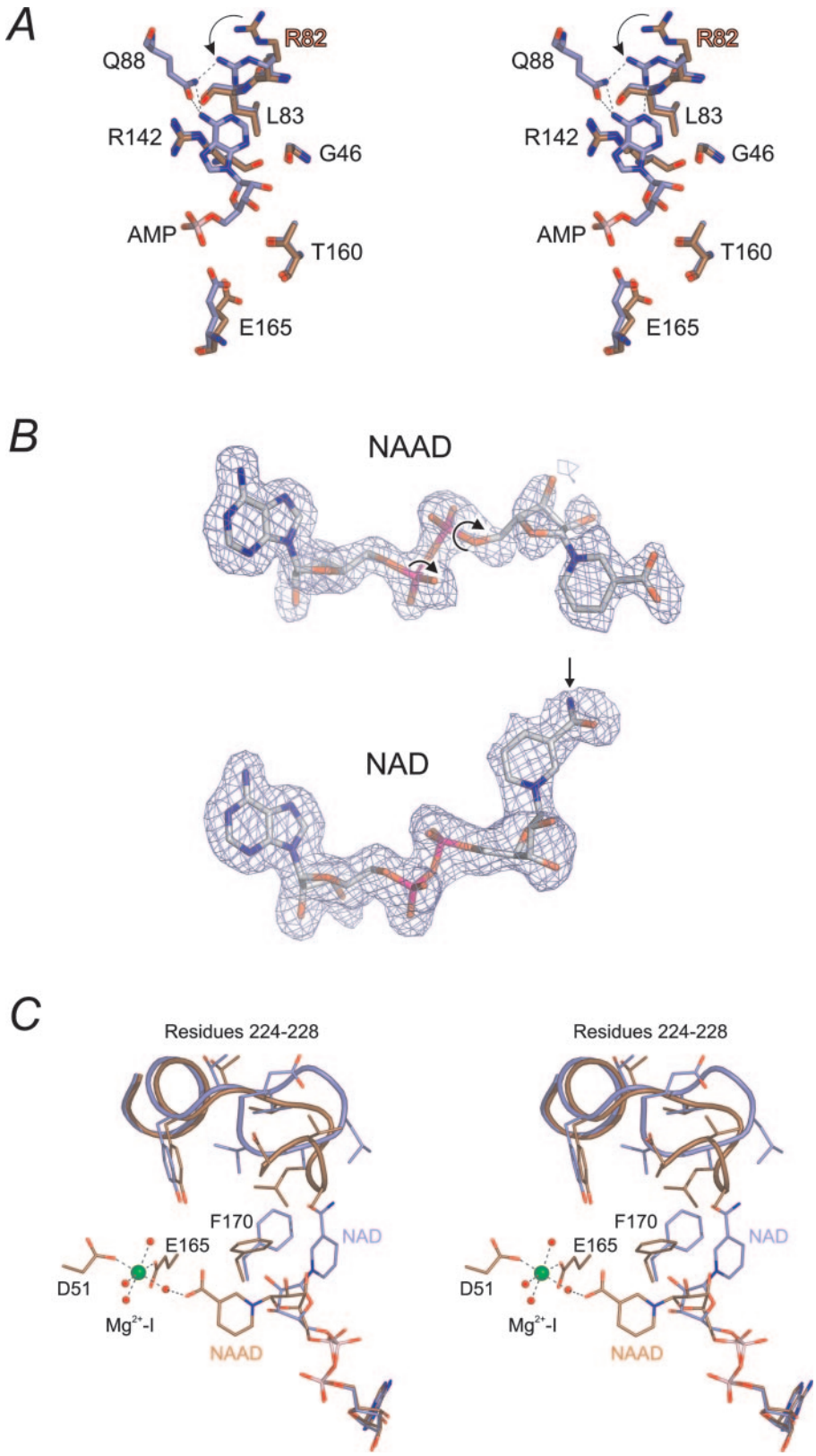

FIG. 5. **Structural rearrangements.** *A*, close-up stereo view of the ATP binding pocket of the *eco*NADS apoenzyme (carbon atoms are in *brown*, and other atoms are colored as described in the legend to Fig. 4) superimposed onto the same region of the AMP complex structure (carbons in *light blue*). Residues lining the binding pocket are labeled in *single letter* style, and Arg-82 (*R82*) is *highlighted*. The *arrow* indicates repositioning of the Arg-82 side chain upon nucleotide binding. The *dashed lines* indicate hydrogen bonds of Arg-82 and of Gln-88 to the adenine base of AMP. *B*, $F_o - F_c$ difference omit map contoured at the 2.5 σ level with a radius of 3 Å around NAAD (*top*) and NAD (*bottom*). The cofactors are shown as *sticks*. *Arrows* around NAAD bonds indicate the main rotations necessary to produce the NAD conformation. The *arrow* in NAD indicates the nitrogen of the amide group introduced in the course of the reaction. *C*, comparison of the NAAD/NAD binding pocket when complexed with NAD (carbon atoms and backbones traces in *light blue*) and when complexed with NAAD (carbon atoms and backbones traces in *brown*) after global superpositioning of the enzyme structures. Other atoms are color-coded as above. Mg^{2+}-I is indicated as a *green sphere* coordinated to the Asp-51 and Glu-165 carboxylate groups and to water molecules (*small red spheres*). One water molecule also hydrogen bonds to the carboxylate of NAAD (*dashed line*). The different conformations of regions 224–228, C-terminal of the disordered loop P2, are indicated by the backbone traces with side chains.

stabilize the nicotinysyl of bound NAAD. These interactions are not seen in *eco*NADS. Supported by the crystal packing (see above), these interactions may therefore contribute to the fixation of loop P2 in *bsu*NADS structures. Interestingly, the C-terminal part of loop P2 also participates in substrate binding in *bsu*NADS. It is involved in the interaction with the nicotinysyl moiety of NAD-adenylate in the *Bacillus* enzyme (PDB code 1KQP). The diol of the nicotinysyl ribose hydrogen bonds to the carboxyl group of Glu-223. Glu-223 is substituted by alanine in the *E. coli* enzyme, which consequently loses the interaction site to the nicotinysyl ribose.

DISCUSSION

In the present manuscript, we presented the high resolution crystal structures of *eco*NADS as well as the structures of the enzyme with various substrates and products. The ensemble of

structures encompasses the first co-crystal structure of a NADS with its enzymatic product, NAD. The structures confirm and significantly expand the picture that has emerged from the structural studies of *bsu*NADS and provide evidence for a wide ranging conformational plasticity in this enzyme family. This plasticity manifests itself in (i) structural reorganizations upon binding of different substrates, (ii) a conformational cross-talk between the ATP binding site and the NAAD/NAD binding pocket, and (iii) conformational adjustments during substrate conversion.

Flexible Elements Mediate Structural Reorganizations upon Substrate Binding—The mode of ATP binding appears to be largely invariant between *E. coli* and *B. subtilis* NADS. In both enzymes, loop P1 becomes fixed upon nucleotide binding to the ATP pocket and thus functions as an evolutionarily conserved lid for the ATP binding site. However, a significant difference between the two enzymes is seen in residue Arg-82, which undergoes side chain reorganization upon ATP or AMP+PP_i binding in *eco*NADS, whereas its ATP-bound conformation is preformed in the *bsu*NADS apoenzyme. Thus, Arg-82 represents a hitherto unrecognized dynamical part of the ATP binding site in addition to loop P1.

Different from loop P1, the P2 loop is disordered in all structures of *eco*NADS presented herein. In contrast, it is ordered in various *bsu*NADS structures, where several of its residues engage in direct or indirect contacts to the substrates ATP and NAAD. In its fixed conformation in *bsu*NADS, both the N- and the C-terminal ends of the P2 loop are involved in substrate binding. At the N terminus, the backbone carbonyl of $Thr\text{-}208^{bsu}$ coordinates to Mg^{2+}-II in the ATP pocket. In addition, residues $Ala\text{-}209^{bsu}$ and $Leu\text{-}211^{bsu}$ participate in the positioning of the nicotinysyl moiety of NAAD (15). At the C terminus, both side chain carboxyl oxygens of $Glu\text{-}223^{bsu}$ hydrogen bond to O-2′ and O-3′ of the nicotinysyl ribose of nucleotides in the NAAD/NAD pocket. The highly similar sequence of the loop in *eco*NADS and the similar modes of substrate binding suggest that P2 can interact in a similar fashion with the substrates in the *E. coli* protein, except for $Glu\text{-}223^{bsu}$ (which is replaced by alanine), but that these substrate interactions are transient. Thus, the main function of loop P2 seems to be the mediation of access to the substrate binding pockets and perhaps shielding them from the environment in the course of the reaction. Complete ordering of this loop in *bsu*NADS structures seems to be observed, because it is supported by favorable crystal lattice contacts.

ecoNADS Dynamics in Response to Substrates and Products—Our data provide the first co-crystal structure of a bacterial NADS in complex with the reaction product, NAD. We have shown that the nicotinysyl moiety of enzyme-bound NAD exhibits higher flexibility than the adenosyl portion and prefers a conformation, which is different from that of NAAD. The conformational difference in the substrate and product coincides with alternate conformations of Phe-170 and residues 224–228 following the C-terminal end of the disordered loop P2. Phe-170 stacks on the nicotinysyl ribose of NAAD and on the nicotinamide ring of NAD in the co-crystal structures. The conformation of residues 224–228 in the NAAD complex sterically interferes with the conformation of bound NAD (Fig. 5*C*). These observations suggest a structural reorganization prior to or accompanying product release. Catalysis requires an orientation of nicotinic acid toward the ATP binding site (14). We speculate that product release requires a torsion within NAD, which in turn necessitates the reorganization of Phe-170 and the P2 loop. A possible trigger for this reorganization may be the Mg^{2+}-I ion. In contrast to the previously reported complex structure of *bsu*NADS with NAAD (15), Mg^{2+}-I is present in our *eco*NADS-NAAD co-crystal structure. The nicotinysyl carboxylate group of NAAD hydrogen bonds to a water of the Mg^{2+}-I coordination sphere. On the other hand, NAD in the form V structure points away from the Mg^{2+}-I site. Thus, Mg^{2+}-I seems to act as an orientation device for the NAAD nicotinysyl moiety, which is activated by adenylyl transfer from ATP in the course of the reaction. Because Mg^{2+}-I under physiological conditions presumably binds to the enzyme in complex with ATP, it prepares the NAAD conformation for this adenylyl transfer when the ATP pocket is ready to deliver the AMP moiety.

The data presented herein for *eco*NADS, including the conservation of the mode of substrate and metal ion binding, are in general agreement with the reaction mechanism described for *bsu*NADS (16), suggesting that it is conserved for bacterial NADSs. However, our ensemble of *eco*NADS structures allows us to expand the mechanism to structural changes taking place in the enzymes upon substrate conversion. We have found that the active center of *eco*NADS exists in different conformations depending on the occupation of the ATP and NAAD/NAD binding sites. We refer to these conformations as the catalysis (or C-) state and the substrate/product exchange (or E-) state. The C-state is displayed in three of our crystal structures (forms II, III, IV), *i.e.* when *eco*NADS is complexed with AMP, AMP+PP_i, or NAAD. The E-state predominates in the apoform of *eco*NADS (form I) and in the complex with NAD (form V). The two states are distinguished by three major features: (i) the side chain conformation of Phe-170, (ii) the conformation of the P2 loop as represented by its C-terminal extension, comprising residues 224–228, and (iii) the occupation of the first magnesium site (Mg^{2+}-I). The two states reflect the structural requirements in pursuing two interdependent processes. The E-state allows substrate binding and product release, and the C-state provides the environment for adenylation and amidation of the substrate NAAD. As described above, Mg^{2+}-I may be the element crucial for switching between the two states, because it seems to orient the NAAD nicotinysyl moiety. Following the enzymatic reaction, AMP, PP_i, and Mg^{2+}-I are released, shifting the equilibrium toward the E-state.

The NAAD/NAD Binding Pocket May Be a Target Site for Future Design of Species-specific Antibiotics—NADS has been proposed to be a promising target for the development of antibiotics to cure *e.g.* anthrax (17, 18). Knowledge of the results of structural comparisons among NADS from different organisms may allow development of inhibitory compounds that exhibit organism specificity. Although the structures of *eco*NADS expectedly revealed a similar overall fold as *bsu*NADS (Figs. 3 and 4*A*), significant structural differences can be observed in detail. In particular, although the architectural alterations in the NAAD/NAD binding sites of *E. coli* and *B. subtilis* NADS do not affect the binding of the natural substrate, their chemically quite different makeup may provide a handle for specific inhibitor design (Fig. 4*C*).

In contrast to bacterial NADSs, which use exclusively ammonia as the amide donor (5, 7), NADS1 from human uses both ammonia and glutamine (11) (the ammonia-specific human NADS2 was later found to derive from a bacterial contamination (9)). Although many catalytic residues are invariant, human NADS1 contains several amino acid substitutions and peptide insertions at the ATP and the NAAD/NAD binding sites (Fig. 2). These differences confirm the suitability of the NADS enzymes for the design of antibiotics, because it should be possible to alleviate side effects in humans.

Acknowledgments—We thank Petra Birle and Tatjana Krywcun for help in enzyme preparation and crystallization, Dr. Hans-Georg Beisel and Dr. Peter Hof for initial help in structure solution, and Prof. Dr. Herbert Jäckle for support in data analysis.

REFERENCES

1. Rizzi, M., and Schindelin, H. (2002) *Curr. Opin. Struct. Biol.* **12,** 709–720
2. Preiss, J., and Handler, P. (1958) *J. Biol. Chem.* **233,** 488–492
3. Preiss, J., and Handler, P. (1958) *J. Biol. Chem.* **233,** 493–500
4. Spencer, R. L., and Preiss, J. (1967) *J. Biol. Chem.* **242,** 385–392
5. Nessi, C., Albertini, A. M., Speranza, M. L., and Galizzi, A. (1995) *J. Biol. Chem.* **270,** 6181–6185
6. Willison, J. C. (1992) *J. Bacteriol.* **174,** 5765–5766
7. Willison, J. C., and Tissot, G. (1994) *J. Bacteriol.* **176,** 3400–3402
8. Cantoni, R., Branzoni, M., Labo, M., Rizzi, M., and Riccardi, G. (1998) *J. Bacteriol.* **180,** 3218–3221
9. Bieganowski, P., and Brenner, C. (2003) *J. Biol. Chem.* **278,** 33056–33059
10. Bieganowski, P., Pace, H. C., and Brenner, C. (2003) *J. Biol. Chem.* **278,** 33049–33055
11. Hara, N., Yamada, K., Terashima, M., Osago, H., Shimoyama, M., and Tsuchiya, M. (2003) *J. Biol. Chem.* **278,** 10914–10921
12. Rizzi, M., Nessi, C., Mattevi, A., Coda, A., Bolognesi, M., and Galizzi, A. (1996) *EMBO J.* **15,** 5125–5134
13. Rizzi, M., Nessi, C., Bolognesi, M., Coda, A., and Galizzi, A. (1996) *Proteins* **26,** 236–238
14. Rizzi, M., Bolognesi, M., and Coda, A. (1998) *Structure (Camb.)* **6,** 1129–1140
15. Devedjiev, Y., Symersky, J., Singh, R., Jedrzejas, M., Brouillette, C., Brouillette, W., Muccio, D., Chattopadhyay, D., and DeLucas, L. (2001) *Acta Crystallogr. Sect. D* **57,** 806–812
16. Symersky, J., Devedjiev, Y., Moore, K., Brouillette, C., and DeLucas, L. (2002) *Acta Crystallogr. Sect. D* **58,** 1138–1146
17. Sutherland, S. (2003) *Drug Discov. Today* **8,** 335–336
18. Velu, S. E., Cristofoli, W. A., Garcia, G. J., Brouillette, C. G., Pierson, M. C., Luan, C. H., DeLucas, L. J., and Brouillette, W. J. (2003) *J. Med. Chem.* **46,** 3371–3381
19. Schoepfer, R. (1993) *Gene* **124,** 83–85
20. Otwinowski, Z., and Minor, W. (1996) *Methods Enzymol.* **276,** 307–326
21. Navaza, J. (2001) *Acta Crystallogr. Sect. D* **57,** 1367–1372
22. Brunger, A. T., Adams, P. D., Clore, G. M., DeLano, W. L., Gros, P., Grosse-Kunstleve, R. W., Jiang, J. S., Kuszewski, J., Nilges, M., Pannu, N. S., Read, R. J., Rice, L. M., Simonson, T., and Warren, G. L. (1998) *Acta Crystallogr. Sect. D* **54,** 905–921
23. McRee, D. E. (1999) *J. Struct. Biol.* **125,** 156–165
24. Laskowski, R. A., MacArthur, M. W., Moss, D. S., and Thornton, J. M. (1993) *J. Appl. Crystallogr.* **26,** 283–291
25. Collaborative Computational Project, N. (1994) *Acta Crystallogr. Sect. D* **50,** 760–763
26. Jones, S., and Thornton, J. M. (1996) *Proc. Natl. Acad. Sci. U. S. A.* **93,** 13–20
27. Wallace, A. C., Laskowski, R. A., and Thornton, J. M. (1995) *Protein Eng.* **8,** 127–134